R. de A. A. Lima, D. Rocca, H.R. M. Da Costa, J.P. B. de Sousa, P. Bettini, G. Sala, M.D. Banea
Interfacial Adhesion Between Embedded Fibre Optic Sensors and Epoxy Matrix in Composites
Journal of Adhesion Science and Technology, Vol. 33, N. 3, 2019, p. 253-272
doi:10.1080/01694243.2018.1537053

Interfacial adhesion between embedded fibre optic sensors and epoxy matrix in composites

R. A. A. Lima[1], D. Rocca[2], H. R. M. Da Costa[1], J. P. B. de Sousa[1], P. Bettini[2], G. Sala[2], M. D. Banea[1]

[1] Federal Centre for Technological Education Celso Suckow da Fonseca – CEFET/RJ, Rio de Janeiro – Brazil.

[2] Aerospace Science and Technology Department of Politecnico di Milano – PoliMi, Milan – Italy.

Corresponding author: R. A. A. Lima[1]- e-mail address: rosemere.raal@gmail.com

Interfacial adhesion between embedded fibre optic sensors and epoxy matrix in composites

Fibre optic (FO) sensors are becoming increasingly popular for different applications in structural monitoring. Among their excellent properties, a strong interest for this type of sensors are represented by the possibility of embedding FOs inside composite components. In this case, one of the factors that significantly influence the efficiency of the whole Structural Health Monitoring (SHM) system is the interfacial adhesion between FO sensors and the host material. The main objective of this work is to investigate the interfacial adhesion between embedded fibre optic sensors and epoxy matrix to find the best type of optical fibre to be used in epoxy matrices to produce smart composites. Four types of optical fibres with different diameters and coatings (i.e. polyimide, polyacrylate and ormoceramic) were used. Pull-out tests were carried out and different methods were used to obtain the composite/optical fibre interfacial properties. Finally, an optical microscopy and Scanning Electron Microscopy (SEM) analysis were performed to characterize the fibre/matrix interfaces. It was found that the optical fibre that presented the highest energy required for interface rupture and, consequently, less invasiveness to the host material was the ormoceramic fibre with the smallest diameter.

Keywords: Structural health monitoring, fibre optics sensors, Pull-out test, interfacial adhesion.

Introduction

In the last decades, the concern of several industrial sectors regarding the use of the predictive maintenance philosophy based on damage tolerance fatigue approach has increased considerably, in order to improve the reliability of the fabricated structures and to reduce operational and maintenance costs.

In the damage tolerance methodology, structures can operate with cracks and small defects without compromising their safety until repairs or replacements are required. This

type of design philosophy has gained prominence due to the wide use of composite materials, which are orthotropic and therefore present great complexity for the creation of damage prediction models. The SHM consists in the implementation of sensors and / or actuators externally bonded or embedded in the structure, linked to algorithms of detection and propagation of damages, data processing software and filtering of noise and false signals. The integration of sensors and / or actuators into structures gives rise to intelligent structures [1]. The use of intelligent structures, mainly by the aerospace industry, has presented as main advantages the increase in safety and reliability of the components in which they are employed as well as a reduction of the time and maintenance costs.

Among the different types of sensors available for implementation in the SHM Systems, fibre optics (FO) are the most commonly used. The main advantages of FO sensors are their low invasiveness, weight and energy required for operation. Moreover, the Fibre Bragg Grating (FBG) sensors, written inside the core of FOs and commonly used as local sensors, are immune to electromagnetic fields and present multiplexing and real time capabilities [2, 3].

Monitoring systems with fibre optic sensors are used for both damage detection and usage monitoring in a wide range of applications, such as: the study and prediction of crack propagation in adhesive joints [4, 5, 6, 7], strain and displacement monitoring of aeronautical structures [8, 9, 10, 11, 12] and civil infrastructures [13, 14, 15].

The efficiency of structural monitoring systems, especially those using embedded sensors or actuators, strongly depends on the transfer of stresses at the interface between them and the composite material matrix [16, 17, 18]. Thus, the durability prediction of the composite is directly linked to an effective fibre-matrix interfacial adhesion and high

debonding strength, consequently guaranteeing a good transfer of mechanical stresses, greater data accuracy and better fatigue life prediction.

In order to study the interfacial adhesion between fibre optic sensors and the matrix in composite materials, an adaptation of micromechanical tests such as Pull-out, fragmentation and micro bond tests are proposed in the literature, due to the absence of tests dedicated to interfacial analysis between sensors and fibres [19, 20]. Moreover, the most popular and reliable test selected for determining the interfacial shear strength (IFSS) is the Pull-out test [21]. This test consists of a tensile test, in which a single wire, partially embedded in a matrix volume, is pulled until its rupture or complete extraction from the matrix (usually a polymeric one) [22, 23].

Bettini *et al*. [24], studied the interfacial adhesion of two different types of optical fibres embedded in a polymeric matrix through the pull-out test. The polyacrylate FO presented a mixed fracture, the coating failed in both epoxy/coating and coating/cladding interfaces, while the polyimide FO showed only adhesive failures in the cladding/coating interface. The polyimide optical fibre presented better results in comparison with the polyacrylate.

Frank *et al.* [29], analysed the debonding strength of Fibre Bragg Grating sensors with two different coatings, one with acrylic and another with polyimide material, in a polymeric matrix. The pull-out test was used, and it was found that in both cases the coatings had a strong superficial adhesion with the matrix and the failure occurred in the coating/cladding interface.

Chean *et al.* [3], used the Pull-out tests to study the interfacial adhesion of fibre optic sensors in composite materials. The influence of the embedding length, temperature and curing time of the matrix relating to the improvement of interfacial adhesion with the same type of optical fibre was analysed. In all the studied cases, the interfacial debonding

was in the cladding/coating interface characterizing an effective interfacial adhesion between the polymeric resin and the coating of the optical fibre. It was found that the main factor that influences the adhesion between optical fibre/matrix is the cure time of the composite and not the temperature.

There are a limited number of studies in the literature about interfacial adhesion between fibre optic sensors and polymeric matrices. Moreover, these studies are normally related to standard FOs that are coated with polyacrylate or polyimide coating. The importance of interface properties in the performance of SHM systems requires further investigation.

This work has the objective of studying the interfacial adhesion of different types of FO sensors within an epoxy matrix. For this purpose, pull-out tests were performed on more conventional fibre optic samples, with polyacrylate and polyimide coating, as well as a new ceramic coating resistant to high temperatures (Ormocer®). Furthermore, an optical microscopy and SEM analysis were carried out to characterize the fibre/matrix interfaces.

Materials and methods

Materials

Four types of optical fibres with different diameters and coatings were investigated, two of them with conventional polyimide and polyacrylate coatings and two Ormocer® (Organic modified ceramics) coated fibres with different coating diameters and same cladding diameter (see Fig. 1 and Table 1). Apart from the Ormocer® 115 optical fibre, which has a reduced cladding diameter. The Ormocer coated fibres are a new type of high temperature resistant ceramic optical fibre with high numerical aperture whose gratings are inscribed during fibre production, thus eliminating the need for a recoating. The optical fibres were supplied by FBGS Technologies, Germany. It is important to note that

no surface treatment will be done on the fibres to alter their surface, therefore only the influence of the different diameters and coating types on the fibre optic / matrix interfacial adhesion will be analysed.

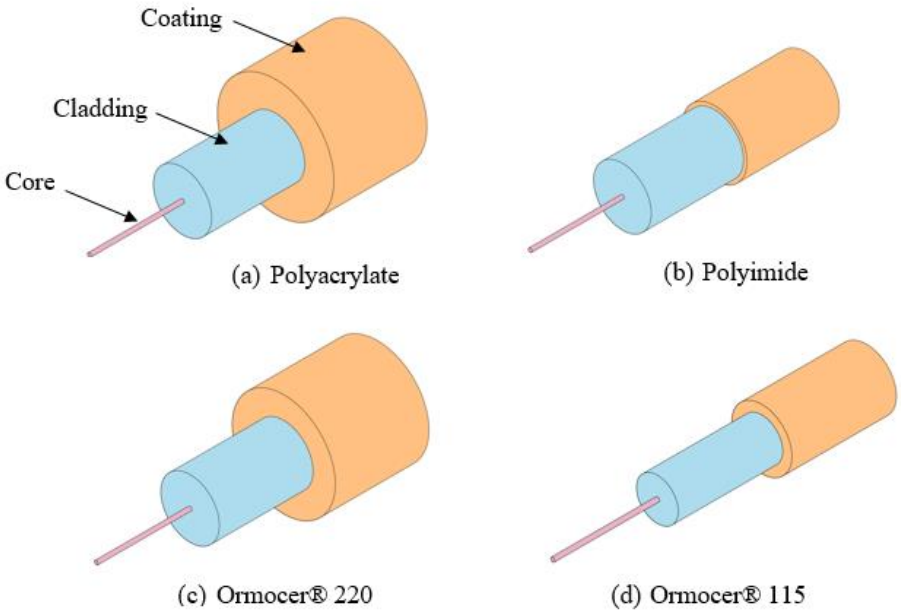

Figure 1: Types of optical fibres. (a) Polyacrylate, (b) Polyimide, (c) Ormocer® 220 and (d) Ormocer® 115.

Table 1: Types of optical fibres.

Types of coating	Diameter cladding (µm)	Diameter coating (µm)	Coating thickness (µm)
Polyacrylate	125	250	125
Polyimide	125	140	15
Ormocer® 220	125	220	95
Ormocer® 115	80	115	35

An epoxy resin E-227 (PROCHIMA, England) was used to produce the specimens with a total cure time of 5 hours at 80 ° C.

Samples production

Due to the great difficulty imposed by the optical fibre dimensions, resin viscosity and the need for a good surface finish of the polymer matrix blocks, a specific mould to produce the specimens was designed and manufactured as can be seen in Fig. 2.

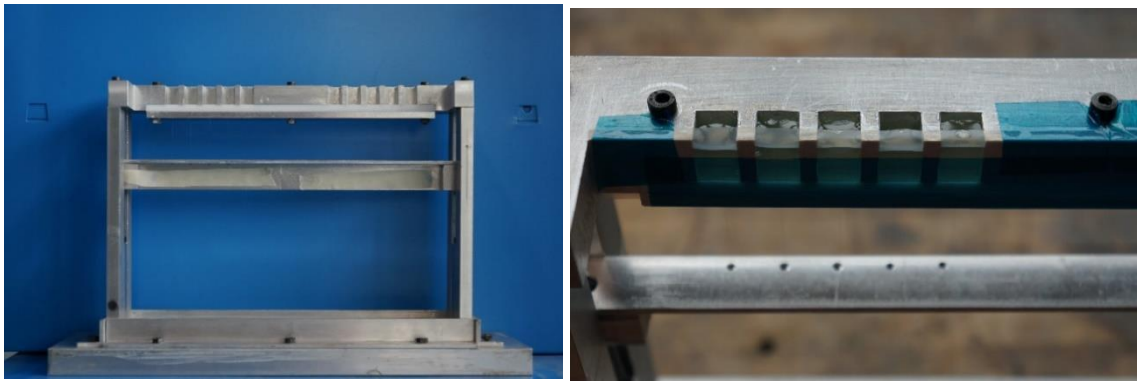

(a) (b)

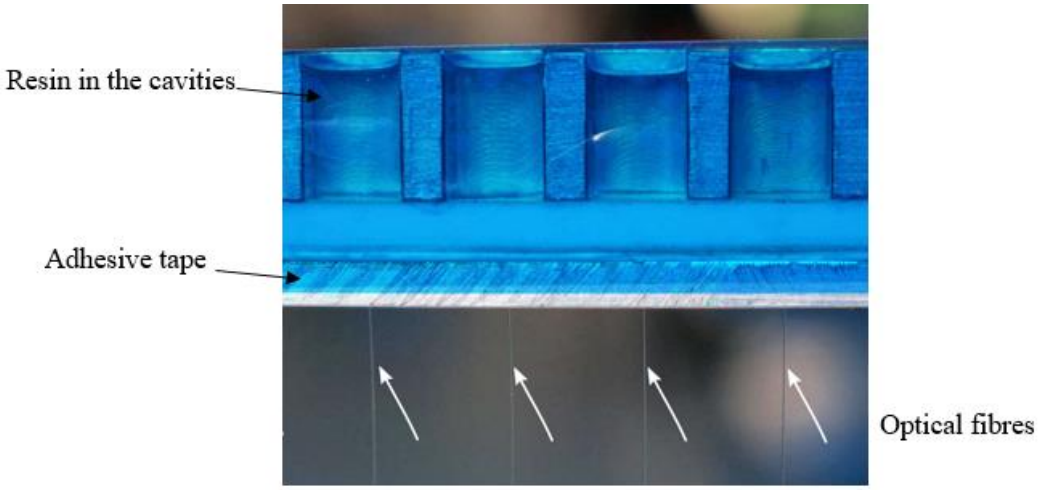

(c)

Figure 2: Mould for production of samples. (a) Pull-out mould (b) mould top view and (c) mould detail.

The fabrication of the test specimens was a delicate operation, due to the fragility of the optical fibres. First, the fibres were cut with a total length of 90 mm and cleaned with alcohol to avoid contaminations. After that, the optical fibres were inserted in the mould with different embedded lengths. At this stage, the open side of the plate was closed with

a high temperature resistant tape, covering the cavities, such that they are only accessible through the upper part of the mould, where the resin was applied.

After the curing cycle, special tabs were applied at the free end of the optical fibres in order to attach the testing machine clamps. The tabs were made of fibreglass and presented an internal V-groove in which the FO could remain aligned with the load direction during the test; tabs were bonded to the FO by a LOCTITE Hysol® 3425 adhesive (LOCTITE - Industrial Adhesives and Sealants, England). Figure 3 shows a pull-out sample.

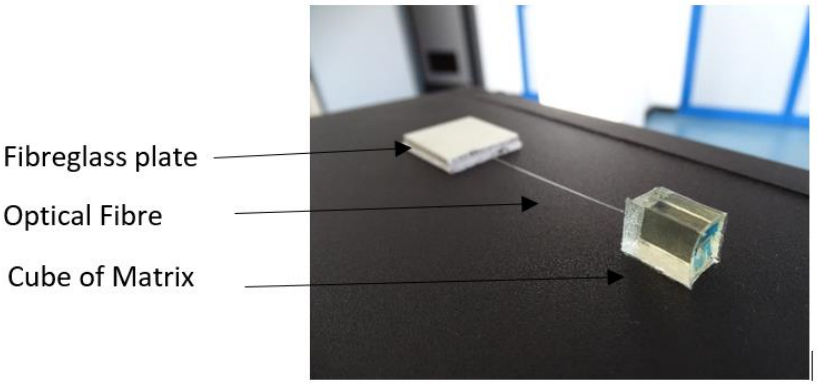

Figure 3: Pull-out samples.

Methods

Technological requirements

For the execution of the pull-out test some prerequisites should be considered, such as the type of fixation of the specimens in the test machine and the regularity and standardization of the specimens. Another important factor is the absence or minimization of defects in the resin and, consequently, reduction of undesirable stress on the fibres.

There are two ways of fixing the specimens on the traction machine: Restrained Top Constrain (RTC) and Fixed Bottom Constrain (FBC). The type of grip chosen was the RTC because this configuration ensures that the force is being applied directly to the fibre, as well as assuring the orthogonality between the upper face of the resin block and the direction of the tensile forces.

Pull-out tests

To carry out the pull-out tests it was necessary to manufacture a specific clamp to apply the tensile load following the RCT method. This clamp, made of fiberglass, is shown in the Figure 4. The machine used for the test was an Instron 4302 with 1 kN load cell and displacement velocity used was equal to 0.5 mm / min (see Fig 4).

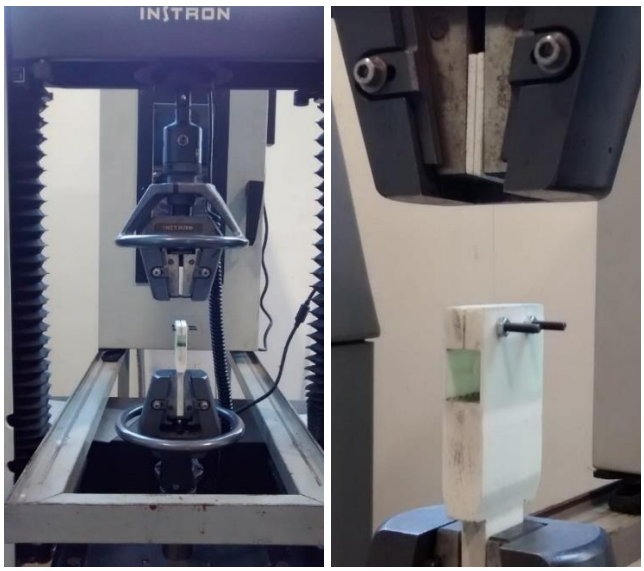

Figure 4: Pull-out test set-up.

Microscopy analysis

A visual and optical microscopy analysis were performed to determinate the type of interfacial failure that occurred and its failure behaviour. Also, a SEM analysis was

performed on the fracture surface of the matrix cube samples using a high-resolution Scanning Electron Microscopy, Carl ZEISS EVO MA 10, at the Multiuser Laboratory of Electronic Microscopy (LMME) of the Fluminense Federal University (UFF), Rio de Janeiro – Brazil. The samples were coated with a thin carbon film, using a Sputter Coater equipment (Materials Laboratory at CEFET/RJ) prior to examination.

In order to verify the influence of the morphology of the optical fibres on the interfacial adhesion between fibre/matrix, they were analysed in the JSM - 7100 F - JEOL electronic microscope, of the Nano multiuser laboratory of manufacture and characterization of nanomaterials, NANOFAB, linked to the State University of Rio de Janeiro - UERJ. The fibres were fixed to the sample holder through a conductive tape, in such a way that a conductive coating was not necessary. The velocity of the electrons used for the analyses was 10 V for all types of optical fibres.

Pull-out data analysis

Force and displacement will be recorded throughout the pull-out test and knowing the geometry of the fibre it is possible to calculate the interfacial resistance between fibre and matrix (τ_{ISS}). Several definitions for the average shear strength for the Pull-out test were presented in the literature, among which the first and probably more widespread was determined by Kelly *et al*. [22], by equation (1).

$$\tau_{ISS} = \frac{F_{max}}{(\pi * d * l_e)} \quad (1)$$

Where F_{max} is the maximum force, d represents the diameter of the wire and l_e the embedded length.

In fact, the interfacial resistance is not linear and presents its maximum value in the free end just before the embedding. In this area the resin enters the plastic regime until a crack is created in the interface and this mechanism of crack propagation repeats until the complete rupture of the interface and fibre extraction [25, 26].

An important concept used in the Pull-out test is the critical fibre breaking length, which represents the minimum fibre length for the failure to occur at the interface, if the length of embedding is greater than the critical length, breakage occurs in the fibre [26, 27, 28].

Maximum interfacial strength

A more refined model for the analysis of interfacial adhesion considering more than the length of embedding as the total length of the process was described by Nairn, *et al*. [25].

The first step consists of the debonding force (FD), which identifies the force of the beginning of the interfacial failure, usually associated with a variation of the elastic modulus of the specimen or the first peak of maximum force during the test. The strain to debonding (τ_d) can be defined by the following equation (2):

$$\tau_d = \frac{F_D}{\pi d l_e} \tag{2}$$

If there were no changes in the modulus of elasticity in the specimen, F_D = F_{max} was adopted. However, the calculation of the resistance at the interface is not a simple process, since even in the 1D models depend on τ along the length of the fibre. Thus, it is assumed that the rupture will occur due to a specific critical effort, from which we can determine the debonding force, according to equation (3).

$$F_D = \frac{\pi d \tau_{ult}}{\beta} \tanh(\beta l_e) - \pi (d/2)^2 \sigma_T tanh(\beta l_e) \tanh(\frac{\beta l_e}{2}) \tag{3}$$

σ_T represents the radial compression stress due to thermal contraction of the resin surrounding the fibre, while β represents the shear-lag, which can be calculated from equation 4, proposed by Nairn, J.A *et al*., [25].

$$\beta^2 = \frac{2}{(\frac{d}{2})^2 E_1 E_2}\left(\frac{E_1V_1+E_2V_2}{\frac{V_2}{4G_1}+\frac{1}{2G_2}\left(\frac{1}{V_2}ln\frac{1}{V_2}-1-\frac{V_2}{2}\right)+\frac{V_2}{(\frac{d}{2})D_S}}\right) \quad (4)$$

In which the two volumetric fractions were defined $V_1 = r_1^2/r_2^2$ e $V_2 = 1 – V_1$, respectively, whereas D_S characterizes the degree of imperfections of the interface between the two cylinders considered. The case in which D_S tends to infinity indicates the perfect continuity between the surfaces in contact, while D_S equals zero means the complete rupture of the interface. For this analysis, the adhesion between interfaces was considered perfect.

Substituting equation (4) into (3) gives:

$$\tau_D = \left(\tau_{ult} - \frac{\beta r_1}{2}\sigma_T tanh\left(\frac{\beta l_e}{2}\right)\right)\frac{\tanh \beta l_e}{\beta l_e} \quad (5)$$

In this step, it is necessary to determine the value of r_2. According to the theory proposed by Nairn [25], r_2 corresponds to the external radius of the cylinder formed by the surface of the matrix.

The Progress of interfacial shear stress along the length of the fibre

An alternative to the previous model is proposed, in which a one-dimensional model of the mean axial stress in the fibre is used as a function of the z-coordinate (along with its length). It is possible to make some considerations about the non-complete elasticity

matrix, presented in the literature [24, 25, 27]. The axial tension along the length of the fibre can be determined by equation (6).

$$\frac{\langle\sigma_1\rangle}{\langle\sigma_{2\infty}\rangle} = 1 - \frac{\langle\sigma_{2\infty}\rangle V_2}{\langle\sigma_{1\infty}\rangle V_1}\frac{\cosh\beta z}{\cosh\beta l_e} \quad (6)$$

In which, the loads tending to infinity are defined according to equation (7).

$$\sigma_{1\infty} = \frac{F}{A_1} \qquad \sigma_{2\infty} = \frac{F}{A_2} \quad (7)$$

From the axial stress progression, it is possible to determine the shear stress of the interface through the equilibrium equation of the fibre element, equation (8).

$$\frac{\partial\langle\sigma_1\rangle}{\partial z} = -\frac{2\tau_{rz}}{r_1} \quad (8)$$

Interfacial critical energy

Jiang, *et al*. [23], proposes that the energy introduced during the pull-out test is dissipated because of interface rupture due to deformation phenomena of the fibre and matrix or to the friction generated in the wall of the matrix during fibre extraction. Thus, the energy balance can be determined by equation (9).

$$\frac{1}{2\pi r}\frac{\partial U}{\partial\alpha} \geq G_C + \frac{1}{2\pi r}\frac{\partial W_f}{\partial\alpha} \quad (9)$$

In which U represents the total elastic energy of accumulated deformation in the system, α is the detached length and W_f corresponds to the work of the frictional force of the fibre region in contact with the matrix, G_C represents the critical energy of interfacial rupture that can be used as an index of interfacial adhesion between fibre / matrix or cladding / coating. The pull-out test specimens can be divided into three parts:

- Zone 1: z < 0

It is the region on the outside of the matrix, in which only the deformation energy of the optical fibre acts;

- Zone 2: $0 < z < \alpha$

It is the characteristic region of crack propagation α, in which the energy present is due to deformation of the matrix and the fibre, besides the friction present due to the extraction process;

- Zone 3: $\alpha < z < l_e$

It corresponds to the length of the fibre to which the matrix is still adhered, in which the energy is dissipated due to the compression of the matrix and the rupture of the interface.

Thus, Equation 9 can be rewritten by specifying each zone, according to equation (10).

$$\frac{\partial U_1}{\partial \alpha} + \frac{\partial U_2}{\partial \alpha} + \frac{\partial U_3}{\partial \alpha} \geq G_C + \frac{1}{2\pi r} \frac{\partial W_f}{\partial \alpha} \quad (10)$$

From equation (10) it is possible to calculate the force P_c referring to the interface assignment, according to equation (11).

$$P_c = A_1 \frac{\sqrt{B^2 - 4AC} - B}{2A} + fa \quad (11)$$

In which the parameters are defined by the following equations:

$$A = \frac{(1+\alpha)A_1}{2E_1} + \frac{(2+\alpha)A_1 csch^2(ns)}{4E_1} \quad (12)$$

$$B = \frac{(1+\alpha)f\alpha}{E_1} + \frac{(2+\alpha)A_1 csch^2(ns)}{2nE_1} \quad (13)$$

$$C = \frac{f^2(1+v_2)\ln\frac{r_2}{r_1}}{2n\pi E_1} - \frac{(1+\alpha)f^2\alpha^2}{2E_1A_1} - 2nr_1G_1 \quad (14)$$

$$\alpha = \frac{E_1A_1}{E_2A_2} \quad (15)$$

$$n^2 = \frac{E_2}{E_1(1+v_2)\ln(r_2 r_1)} \quad (16)$$

$$s = \frac{l-a}{r_1} \quad (17)$$

Considering the initial instant in which the crack originates, where a = 0, the contribution of the friction($f = 0N/mm$), can be disregarded, and if the tensile force is known, it is possible to determine the critical breaking energy of the G_C interface, through eq. (11).

Results and discussion

Pull-out tests

Representative load-displacement curves of the pull-out test can be seen in Fig. 5.

For the polyacrylate coating fibres (Fig. 5 (a)) an initial peak (interfacial rupture between cladding and coating) was observed, with different values for each test specimen, followed by a decay to a plateau at a constant value of about 1.15N. Such behaviour is attributed to the low mechanical strength of the polyacrylate coating and its plasticity. It is worth mentioning that the friction of the optical fibre inside the resin block during the extraction process contributes to the increase of the pulling force. The fibres coated with polyacrylate showed a maximum pull-out force of 4N.

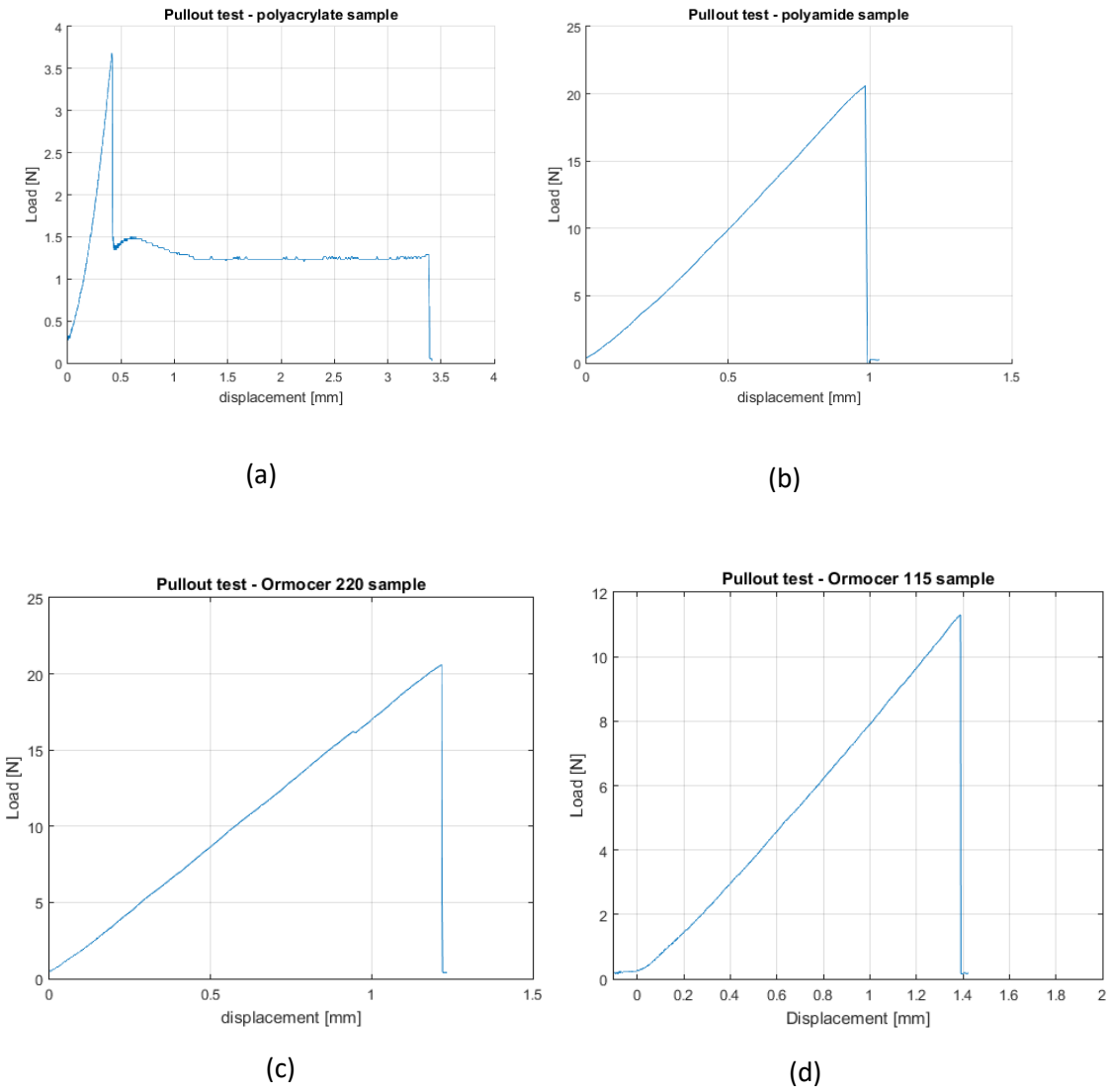

Figure 5: Representative load-displacement curves as a function of fibre type (a) polyacrylate sample, (b) polyimide sample, (c) Ormocer® 220 sample and (d) Ormocer® 115 sample.

Figure 5 (b) shows the characteristic force-versus-displacement curve of the polyimide fibre. In this case, a sudden and well-marked yield is observed after the maximum pull-out force, which in this case was around 20 N. In this fibre typology, two types of interfacial breaks between coating / cladding and coating / matrix were observed, in which the fibres that showed rupture between cladding /coating presented lower maximum pull-

out load. This difference of behaviour characteristic of the test can be explained by the lower tenacity of the polyimide coating, in addition to the smaller coating thickness contributing to its fragility.

The Ormocer coating of diameter 220µm (Fig. 5 (c)) presented very similar results to the polyimide, instantaneous yield followed by zero load, with a complete extraction of the fibre, a characteristic behaviour of Pull-out curves found in previous research [3, 24, 27, 29]. After the extraction of the fibre, coating traces were no longer observed on the surface.

For the same coating, but with a diameter of 115µm (Fig. 5 (d)), the same behaviour as of the 220 µm fibre was observed. However, its reduced diameter gives a greater sensitivity of the fibre in relation to possible imperfections present in the test specimens. In this case, the maximum rupture force of the interface was 10N.

A possible comparison to be made is the maximum breaking strength by length of embedding of the different types of fibres studied, Fig. 6.

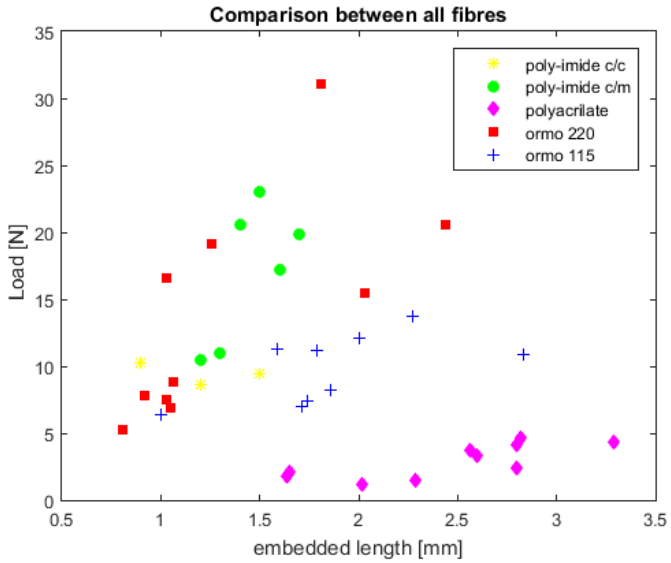

Figure 6: Maximum load (N) x embedded length (mm).

From Fig. 6, it is noted that the polyacrylate coating fibre has the worst results in relation to interfacial adhesion. The other fibres presented similar results, especially the fibres of Ormocer and 115μm in diameter, which presented lower results.

Average interfacial shear strength

Table 2 presents the average interfacial strength for each type of optical fibre obtained according to eq. (1).

Table 2: Average Interfacial Strength

τ_{ISS} (N/mm^2)			
Polyacrylate	Polyimide	Ormocer 220	Ormocer 115
2.96	26.38	25.88	21.48

As can be seen in Table 2, there is no significant difference between the average strength of the polyimide-coated fibres and the Ormocer® - 220 μm fibre. While the Ormocer® - 115 μm fibre presented an excellent result in view of the reduction of its diameter. The polyacrylate fibre presented the worst result, with about 10% of the resistance of the other fibres. Such results are similar to those found by Bettini *et al*., [24].

In this case, the process of breaking the interface, although sudden, is a gradual process that affects a well-defined and limited characteristic length. So, the value of tolerable shear stress is necessarily underestimated.

Maximum interfacial strength

The maximum interfacial shear stress was calculated for each type of fibre and detailed in Table 3.

Table 3: Maximum Interfacial Strength

$\tau_D\ (N/mm^2)$			
Polyacrylate	Polyimide	Ormocer 220	Ormocer 115
46.49	232.60	226.30	389.41

For this method, it is considered that the coating has a perfect adhesion to the matrix, and part of the shear stress is transferred to it. However, the matrix's plasticity was not examined. In this case, the Ormocer® - 115µm fibre presented more significant results regarding the interfacial adhesion, followed by the polyimide and Ormocer® fibres of larger diameter.

Progress of interfacial shear stress along the length of the fibre

Figure 7 represents the progress of the interfacial shear stress along the length of the fibre. Only the first millimetre of fibre embedding was represented since the maximum shear stress lies at the end of the intercession between the fibre and the matrix.

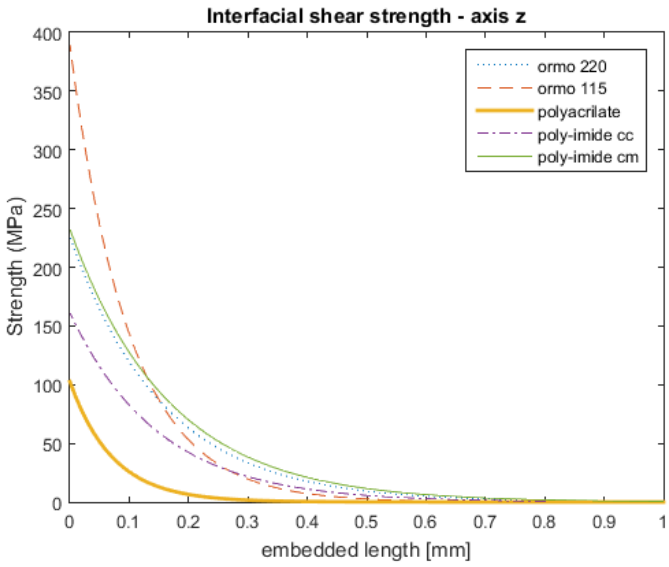

Figure 7: Interfacial Shear Strength (MPa) x embedded length (mm).

It should be noted that the peak values, specified for clarity in Table 3, are the same as those obtained in Fig. 7. Thus, this can also be a verification of the implementation of the two models (maximum interfacial strength and progress of interfacial shear stress).

The next step was to introduce the boundary of the matrix elastic field, which for the sake of simplicity was considered equal to 50MPa. The graph obtained can be seen in Fig 8.

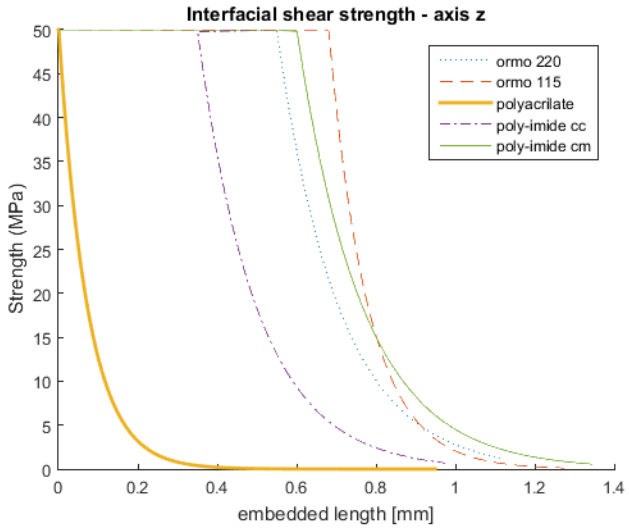

Figure 8: Interfacial shear strength as a function of embedded length.

In this case, the relative behaviour of the interfacial shear stress of the polyacrylate fibre was observed. The larger diameter polyimide and Ormocer fibres present similar behaviour curves. However, the smaller diameter Ormocer fibre presented a slight difference in the progress of the curve, which in the case of fibres with a smaller diameter tends to zero more quickly.

Through the same graph, another consideration is possible: the characteristic length of polyacrylate specimens is, in fact, the smallest of all, and it is precisely for this reason that it has been possible to extract the fibre without any breakage.

Interfacial critical energy

The interfacial critical energy is shown in Table 4. The optical fibre that presented the best fibre / matrix or cladding / coating interfacial adhesion was the Ormocer coating of smaller diameter, which presented a critical energy of rupture about 30% higher than that of the Ormocer 220µm.

Table 4: Interfacial critical energy

$G_c\ (kJ/m^2)$			
Polyacrylate	Polyimide	Ormocer 220	Ormocer 115
0.06	1.21	2.36	3.57

Optic microscopy and SEM analysis

Optical microscopy was used to analyse the surface of the fibre and its coating after the extraction test. The first fibre analysed was polyacrylate (Fig. 9) and the elastic / plastic

behaviour of the polyacrylate coating was observed. The plastic behaviour is confirmed by the presence of a coating fixed in the resin block with a larger length than the initial one characterizing an increased dimensionality due to its plasticity.

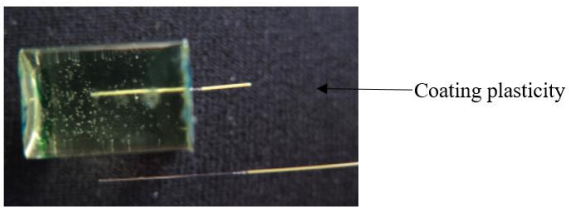

Figure 9: Photo of polyacrylate coating showing plastic behaviour.

The photos of the ormoceramic coated fibres are presented in Fig. 10 (a) and (b). After extraction of the 115µm fibre from the resin block, the cladding is completely exposed, that is, the coating presents an excellent adherence to the epoxy matrix. Part of the coating of the fibre of greater diameter remained adhered to the cladding, indicating a mixed failure between cladding/coating and coating/matrix.

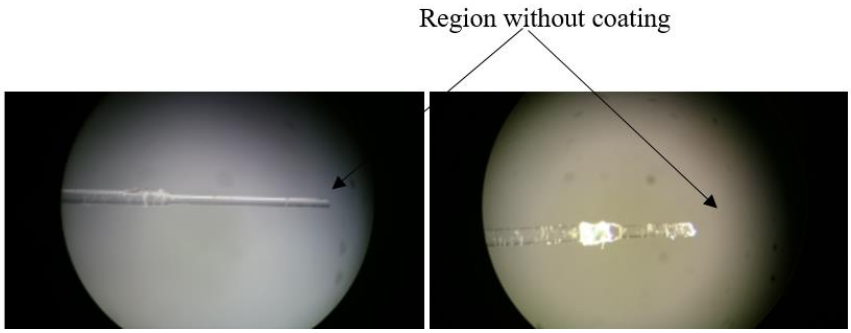

Figure 10: Image of Ormocer® fibres (a) fibre of 115µm and (b) fibre of 220µm.

The polyimide coating fibres presented two distinct interfaces of rupture: in the first one, similar to the behaviour of the ormoceramic fibre, the failure occurred between cladding / coating (Fig. 11 (a)); In the second, the rupture occurs between the coating and the matrix (Fig. 11 (b)). It was also observed that for polyimide fibres with short embedded lengths the failure occurred at the interface coating/matrix, which indicates that the better interfacial adhesion occurs between the coating and matrix with longer embedded lengths.

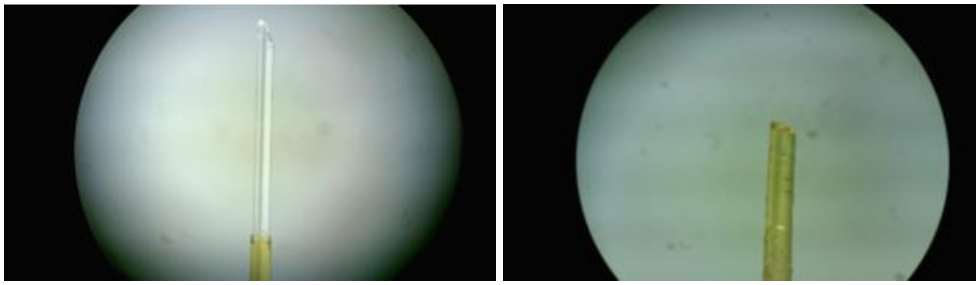

(a) (b)

Figure 11: Image of polyimide fibre (a) interface cladding/coating e (b) interface coating/matrix.

A SEM analysis was used to confirm the presence of the adherent coating on the resin samples, to identify the formation of cracks and their propagation during the tests, as well as analysing the fibre surfaces. The SEM micrographs of the polyacrylate and Ormocer® fibres are shown in Fig. 12.

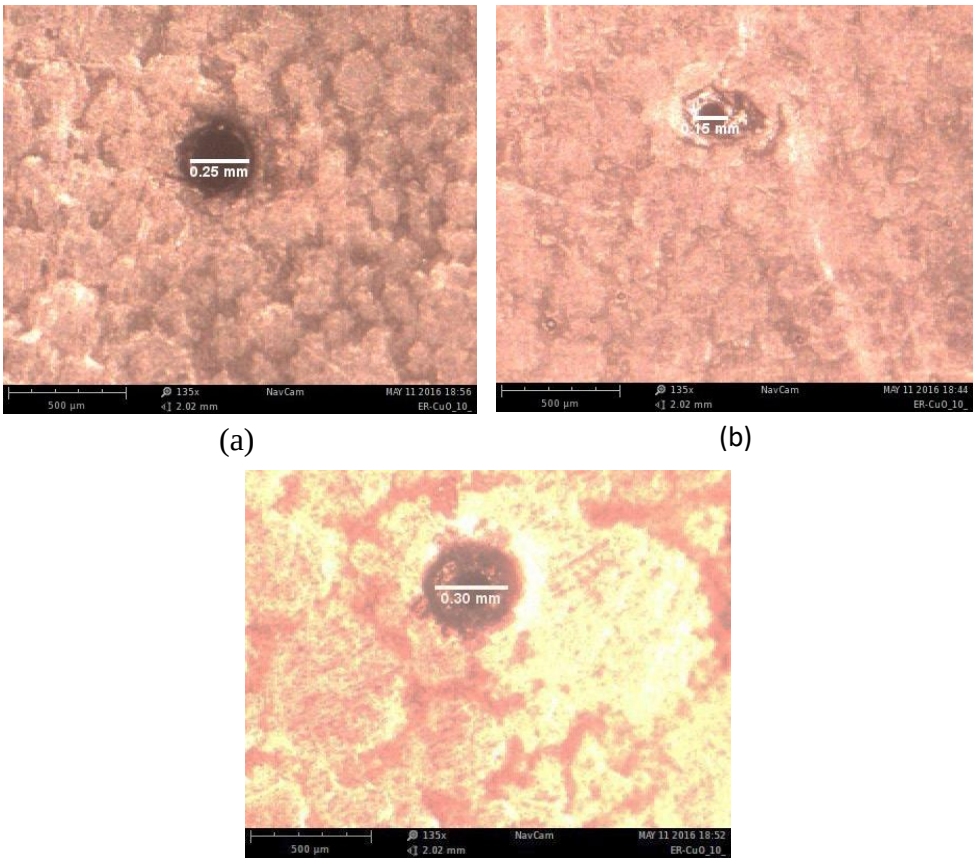

(a) (b)

(c)

Figure 12: SEM image of cavity detail – (a) polyacrylate coating, (b) fibre of 115µm and (c) fibre of 220µm

The images above show the cavities left in the resin cubes after the pull-out tests. It was observed that the cavity left by the polyacrylate coating did not present large variations of the initial sensor diameter. This indicates that there is no presence of burrs and coating accumulation on the surface of the matrix, which can be explained by its elastic/plastic coating characteristics. However, the same cannot be said for the ormoceramic coating which presented a dimensional increase in the cavity region. In order to more accurately verify the behaviour of the Ormocer® coating, the SEM images where increased by 530 times, as shown in Fig. 13.

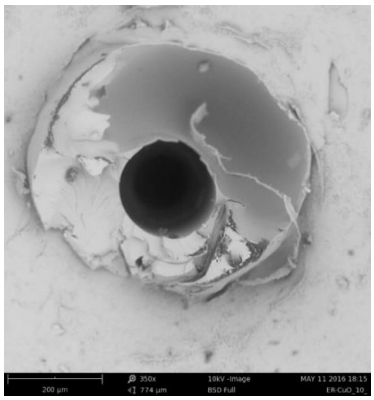

Figure 13: SEM images of cavity detail - 220μm fibre, ormoceramic coating.

From Fig. 13 it is possible to observe the crack propagation that led to the rupture of the cladding / coating interface and the presence of the coating, fully adhered to the surface of the matrix, demonstrating an excellent adhesion between coating and epoxy resin. The presence of burrs, due to the presence of several planes in the enlarged image can be also observed. This is probably due to coating regions which were in contact only with the fibre, and after the fibre extraction the coating remained grouped in the resin cube.

SEM analyses were performed in order to verify the influence of the surface of the optical fibres on the interfacial adhesion between fibre and matrix (see Fig. 14).

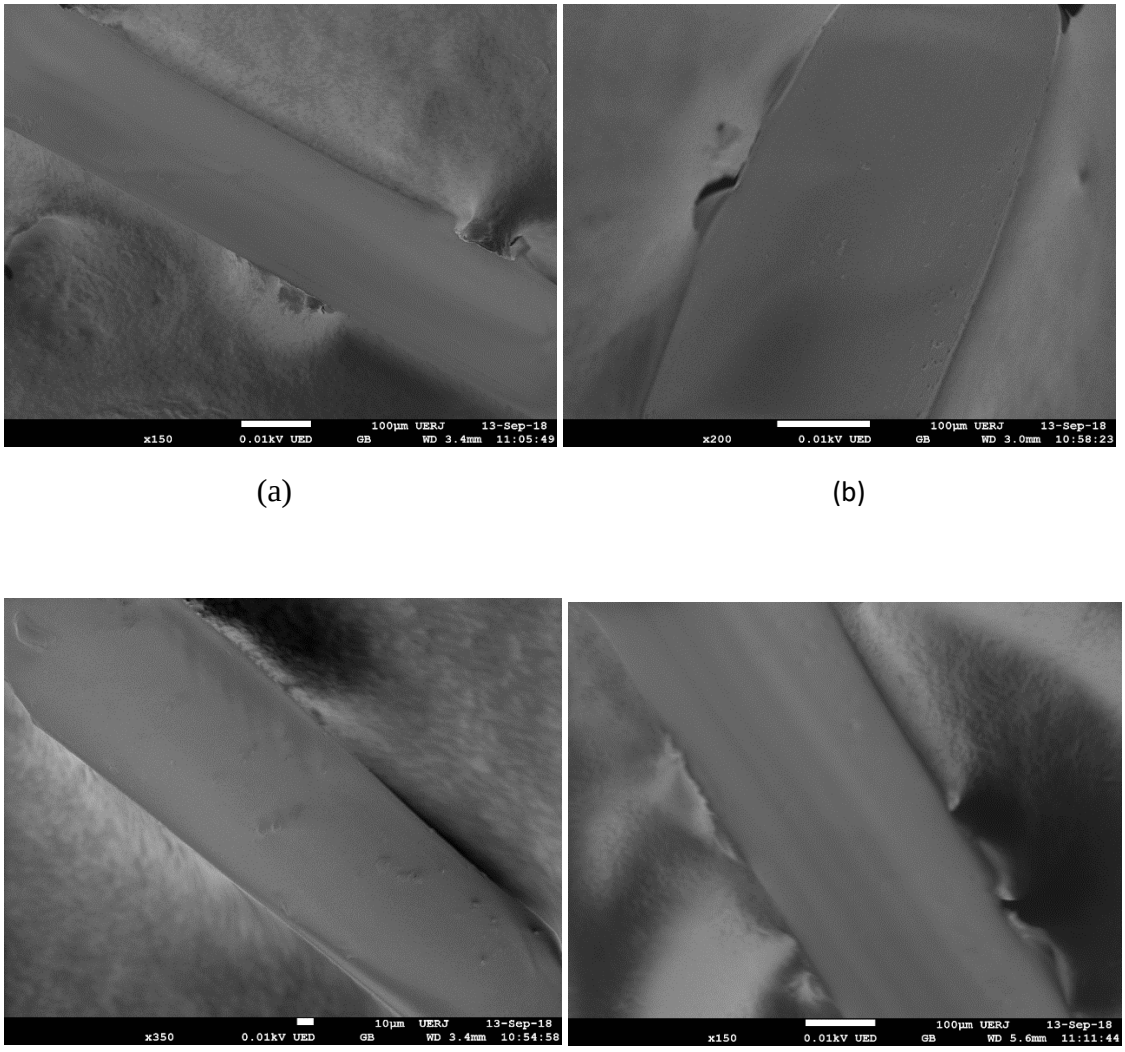

Figure 14: SEM images morphological analyses – (a) polyimide coating, (b) polyacrylate coating, (c) Ormocer® - 115µm and (d) Ormocer® - 220µm.

It can be seen, that the fibre morphology is quite similar, and no significant differences were observed between the surfaces of the different types of coatings. The images indicate good coverage by the coatings on the optical fibres and a smooth surface. Thus, it is possible to conclude that the differences presented in the values of the interfacial critical

energy are directly correlated to the type of coating (polyimide, polyacrylate or Ormocer®) and its adhesion to the matrix.

In summary, the polyimide and polyacrylate fibres presented a similar behaviour to those found in the literature [3, 24, 29]. The fibres showed interfacial rupture between cladding / coating, except for the polyimide fibre that also showed rupture between the coating / matrix interface. The new typologies of optical fibres with ormoceramic coating presented the best results, when considering the energy required for interfacial debonding. The Ormocer® coated fibre - 220μm presented a maximum energy for interfacial rupture of around two times larger than the polyimide fibre, followed by the Ormocer®- 115μm with about triple the debonding energy. In addition, to the reasons mentioned above, which makes the new coating already preferable to the pre-existing ones, the high breaking energy of the fibre interface with 80μm cladding underlines that this is the less invasive type on the host material. Thus, the fibre that presented the best interfacial adhesion between cladding / coating and, therefore, the most suitable for application in the studied matrix is the Ormocer® - 115μm.

Conclusions

In this work, four types of optical fibres with different diameters and coatings (polyimide, polyacrylate and ormoceramic) were studied in order to determine the best type of optical fibre to be used in epoxy matrices for the production of smart composites. It was found that the behaviour of Ormocer coated fibre with a diameter of 220μm significantly approximates the result presented by the polyimide coated fibre, widely used by industry. However, the Ormocer® coated fibres have the advantage of a greater numerical aperture which minimizes the effects of bending loss, high mechanical resistance, does not have

the need of recoating and lower cost. The experimental results did not show a significant difference between the maximum pull-out forces of the polyimide fibres and Ormocer® - 220μm. The polyacrylate fibre presented the lowest values for the maximum pulling force and a characteristic plateau in its load x displacement curves, indicating the plasticity of its coating. Although there is no specific mathematical formulation for determining the critical energy of interfacial rupture between optical fibres and polymer matrices, the adaptations performed have shown plausible results.

The fibre that presented the highest critical breakdown energy of the interface and, therefore, a higher interfacial adhesion was the Ormocer coated fibre of smaller diameter, being, the best recommended fibre for structural monitoring applications in composites that use the studied matrix. In addition, the fibre has a smaller diameter, and consequently, is less invasive.

The microscopy analysis showed the type of interfacial rupture that occurred in the test specimens and verified that in most cases the coatings had an excellent adhesion in the epoxy matrix, with the debonding at the interface between the coating / cladding.

Acknowledgments

The authors would like to thank CAPES for the scholarship through the Sciences without Borders program and FBGS Technology, Germany, for supplying the optical fibres.

References

1. Sala G, Di Landro L, Airoldi A, et al. Fibre optics health monitoring for aeronautical applications. Meccanica. 2015 October 01;50(10):2547-2567. doi: 10.1007/s11012-015-0200-6.
2. Bettini P, Sala G, Di Landro L, et al., editors. Embedded fibre optic techniques for primary structural components: strain and temperature monitoring. proceedings of the 15th European conference on composite materials, ECCM, Padova (It), ICCM; 2012.

3. Chean V, Matadi Boumbimba R, El Abdi R, et al. Experimental characterization of interfacial adhesion of an optical fiber embedded in a composite material. International Journal of Adhesion and Adhesives. 2013 2013/03/01/;41:144-151. doi: https://doi.org/10.1016/j.ijadhadh.2012.11.006.
4. Bernasconi A, Carboni M, Comolli L, et al. Fatigue crack growth monitoring in composite bonded lap joints by a distributed fibre optic sensing system and comparison with ultrasonic testing [Article]. Journal of Adhesion. 2016;92(7-9):739-757. doi: 10.1080/00218464.2015.1123153.
5. Bernasconi A, Kharshiduzzaman M, Comolli L. Strain Profile Measurement for Structural Health Monitoring of Woven Carbon-fiber Reinforced Polymer Composite Bonded joints by Fiber Optic Sensing Using an Optical Backscatter Reflectometer [Article]. Journal of Adhesion. 2016;92(6):440-458. doi: 10.1080/00218464.2015.1043005.
6. Da Silva LFM, Moreira PMGP, Loureiro ALD. Determination of the strain distribution in adhesive joints using Fiber Bragg Grating (FBG) [Article]. Journal of Adhesion Science and Technology. 2014;28(14-15):1480-1499. doi: 10.1080/01694243.2012.698120.
7. Bernasconi A, Carboni M, Galeazzi R, et al., editors. Experiments on distributed fiber optic sensing for fatigue crack growth monitoring of composite adhesively bonded single lap joints. ECCM 2016 - Proceeding of the 17th European Conference on Composite Materials; 2016.
8. Jones TP, Thorvaldsen T, Sagvolden G, et al., editors. Bond strength and performance of optical fibre bragg gratings sensors embedded in composite patch repairs for military aircraft. 8th European Workshop on Structural Health Monitoring, EWSHM 2016; 2016.
9. Grave JHL, Håheim ML, Echtermeyer AT. Measuring changing strain fields in composites with Distributed Fiber-Optic Sensing using the optical backscatter reflectometer [Article]. Composites Part B: Engineering. 2015;74:138-146. doi: 10.1016/j.compositesb.2015.01.003.
10. Tserpes KI, Karachalios V, Giannopoulos I, et al. Strain and damage monitoring in CFRP fuselage panels using fiber Bragg grating sensors. Part I: Design, manufacturing and impact testing [Article]. Composite Structures. 2014;107:726-736. doi: 10.1016/j.compstruct.2013.09.053.
11. Ruzek R, Kudrna P, Kadlec M, et al. Strain and damage monitoring in CFRP fuselage panels using fiber Bragg grating sensors. Part II: Mechanical testing and validation [Article]. Composite Structures. 2014;107:737-744. doi: 10.1016/j.compstruct.2013.09.056.

12. Ciminello M, Bettini P, Ameduri S, et al. Monito-Ring: an Original Fiber Optic System for Morphing Application [Article]. Journal of Intelligent Material Systems and Structures, 2015;26(18):2463-2476. doi: 10.1177/1045389X14568818.
13. Morsy R, Marzouk H, Haddara M, et al. Multi-channel random decrement smart sensing system for concrete bridge girders damage location identification [Article]. Engineering Structures. 2017;143:469-476. doi: 10.1016/j.engstruct.2017.03.040.
14. Nianchun D, Jianming L, Yuejing L, et al., editors. Experimental study on the in-situ stress measurement of Reinforced concrete structure by the ring-hole method with FBG sensor. Structural Health Monitoring 2017: Real-Time Material State Awareness and Data-Driven Safety Assurance - Proceedings of the 11th International Workshop on Structural Health Monitoring, IWSHM 2017; 2017.
15. Nishio M. Quality evaluation of fiber-optic strain data acquired in long-term bridge monitoring [Article]. Sensors and Materials. 2017;29(2):141-152. doi: 10.18494/SAM.2017.1462.
16. Lau K-t, Yuan L, Zhou L-m, et al. Strain monitoring in FRP laminates and concrete beams using FBG sensors. Composite Structures. 2001 2001/01/01/;51(1):9-20. doi: https://doi.org/10.1016/S0263-8223(00)00094-5.
17. Zhou G, Sim LM. Evaluating damage in smart composite laminates using embedded EFPI strain sensors. Optics and Lasers in Engineering. 2009 2009/10/01/;47(10):1063-1068. doi: https://doi.org/10.1016/j.optlaseng.2009.03.004.
18. Bettini P, Riva M, Sala G et al. Carbon fiber reinforced smart laminates with embedded sma actuators-part I: embedding techniques and interface analysis [Article]. Journal of Materials Engineering and Performance. 2009; 18:664-671. doi: 10.1007/s11665-009-9384-z
19. DiFrancia C, Ward TC, Claus RO. The single-fibre pull-out test. 1: Review and interpretation. Composites Part A: Applied Science and Manufacturing. 1996 1996/01/01/;27(8):597-612. doi: https://doi.org/10.1016/1359-835X(95)00069-E.
20. Severin I, Abdi RE, Corvec G, et al. Optical Fiber Embedded in Epoxy Glass Unidirectional Fiber Composite System. Materials. 2014 12/20 (1):44-57. doi: 10.3390/ma7010044. PubMed PMID: PMC5453130.
21. Tomić NZ, Međo BI, Stojanović DB, et al. A rapid test to measure adhesion between optical fibers and ethylene–vinyl acetate copolymer (EVA). International Journal of Adhesion and Adhesives. 2016 2016/07/01/;68:341-350. doi: https://doi.org/10.1016/j.ijadhadh.2016.04.012.

22. Kelly A, Tyson WR. Tensile properties of fibre-reinforced metals: Copper/tungsten and copper/molybdenum. Journal of the Mechanics and Physics of Solids. 1965 1965/12/01/;13(6):329-350. doi: https://doi.org/10.1016/0022-5096(65)90035-9.
23. Jiang KR, Penn LS. Improved analysis and experimental evaluation of the single filament pull-out test. Composites Science and Technology. 1992 1992/01/01/;45(2):89-103. doi: https://doi.org/10.1016/0266-3538(92)90031-W.
24. Bettini P, Di Landro L, Airoldi A, et al. Characterization of the interface between composites and embedded Fiber Optic sensors or NiTiNOL wires. Procedia Engineering. 2011 2011/01/01/;10:3490-3496. doi: https://doi.org/10.1016/j.proeng.2011.04.575.
25. Nairn JA. On the use of shear-lag methods for analysis of stress transfer in unidirectional composites. Mechanics of Materials. 1997 1997/09/01/;26(2):63-80. doi: https://doi.org/10.1016/S0167-6636(97)00023-9.
26. Nairn J. Generalized Shear-Lag Analysis Including Imperfect Interfaces. Vol. 13. 2004.
27. Yue CY, Looi HC, Quek MY. Assessment of fibre-matrix adhesion and interfacial properties using the pull-out test. International Journal of Adhesion and Adhesives. 1995 1995/04/01/;15(2):73-80. doi: https://doi.org/10.1016/0143-7496(95)98740-D.
28. Zhandarov S, Pisanova E, Mäder E, et al. Investigation of load transfer between the fiber and the matrix in pull-out tests with fibers having different diameters. Journal of Adhesion Science and Technology. 2001 2001/01/01;15(2):205-222. doi: 10.1163/156856101743418.
29. Frank A, Nellen PM, Sennhauser U. Characterization of Embedded Optical Fiber Bragg Grating Sensors. MRS Proceedings. 2011;531:397. doi: 10.1557/PROC-531-397.